


Magnetic reshuffling and feedback on superconductivity in UTe_2 under pressureM. Vališka^{1,2}, W. Knafo³, G. Knebel¹, G. Lapertot¹, D. Aoki⁴, and D. Braithwaite¹¹*Univ. Grenoble Alpes, CEA, Grenoble INP, IRIG, PHELIQS, 38000, Grenoble, France*²*Charles University, Faculty of Mathematics and Physics, Department of Condensed Matter Physics, Ke Karlovu 5, Prague 2, 121 16, Czech Republic*³*Laboratoire National des Champs Magnétiques Intenses - EMFL, CNRS, Univ. Grenoble Alpes, INSA-T, Univ. Toulouse 3, 31400 Toulouse, France*⁴*Institute for Materials Research, Tohoku University, Ibaraki 311-1313, Japan* (Received 2 August 2021; revised 10 November 2021; accepted 7 December 2021; published 17 December 2021)

The discovery of superconductivity in the heavy-fermion paramagnet UTe_2 has attracted a lot of attention, particularly due to the reinforcement of superconductivity near pressure- and magnetic-field-induced magnetic quantum phase transitions. A challenge is now to characterize the effects of combined pressure and magnetic fields applied along variable directions in this strongly anisotropic paramagnet. Here, we present an investigation of the electrical resistivity of UTe_2 under pressure up to 3 GPa and pulsed magnetic fields up to 58 T along the hard magnetic crystallographic directions **b** and **c**. We construct three-dimensional phase diagrams and show that, near the critical pressure, a field-enhancement of superconductivity coincides with a boost of the effective mass related to the collapse of metamagnetic and critical fields at the boundaries of the correlated paramagnetic regime and magnetically-ordered phase, respectively. Beyond the critical pressure, field-induced transitions precede the destruction of the magnetically-ordered phase, suggesting an antiferromagnetic nature. By bringing new elements about the interplay between magnetism and superconductivity, our paper appeals for microscopic theories describing the anisotropic properties of UTe_2 under pressure and magnetic field.

DOI: [10.1103/PhysRevB.104.214507](https://doi.org/10.1103/PhysRevB.104.214507)**I. INTRODUCTION**

The recent discovery of superconductivity in the strongly correlated system UTe_2 has sparked enormous interest [1,2]. This orthorhombic compound is a paramagnet with anisotropic magnetic properties [1–5]: the magnetic susceptibility along the *a* axis increases strongly at low temperature, leading to the initial suggestion that the system is very close to ferromagnetic order [1], whereas the other directions are “hard” magnetization axes, with **b** being the hardest at low temperature. But the properties of the superconducting state are the most striking aspect, and in particular the strong enhancement of superconductivity when a magnetic field **H** is applied along the *b* axis [6,7]. In this case superconductivity persists in magnetic fields up to $\mu_0 H_m = 35$ T, where a first-order metamagnetic transition occurs with a large jump of the magnetization [4], a similarly large jump in the residual electrical resistivity of the normal state [8], and the destruction of superconductivity [6,7,9]. Even more remarkably when the field is tilted by about 30° from the *b* axis in the hard **b** – **c** plane, superconductivity re-emerges above $\mu_0 H_m \simeq 40$ T for this angle [6,10]. The extremely high values of the upper critical field H_{c2} compared to the initial superconducting critical temperature ($T_{sc} = 1.6$ K) suggest a probable spin-triplet order parameter, at least in some parts of the phase diagram. This enhancement of superconductivity is very reminiscent of the phenomenon found in the ferromagnetic superconductors URhGe [11] and UCoGe [12]. However, in these

cases the reinforcement of superconductivity, when a field is applied along a hard magnetic axis, is understood as a consequence of the collapse of ferromagnetism, and an enhancement of the ferromagnetic fluctuations have been shown to be responsible for the superconducting pairing [13,14]. This explanation can obviously not be directly transposed to UTe_2 where no sign of magnetic ordering has been found down to very low temperatures [15,16]. Low-dimensional antiferromagnetic fluctuations were reported, suggesting that UTe_2 , whose U ions form a magnetic ladder structure, is subject to antiferromagnetic exchange leading to antiferromagnetic correlations [17,18]. The opening of a gap associated with these antiferromagnetic fluctuations was also observed in the superconducting phase [19,20]. The magnetic properties of UTe_2 are thus associated to its unusual superconducting properties. A full description of the relationship between the two is essential to understand superconductivity in UTe_2 , and may well advance our understanding of magnetically-mediated superconductivity in general.

Applying pressure is the tool of choice to tune magnetism in strongly correlated systems. Often pressure (*p*) can drive a system towards and through a magnetic instability, giving a direct probe of the relationship between magnetism and superconductivity. For UTe_2 it has already been shown that hydrostatic pressure induces an enhancement of T_{sc} by a factor 2, reaching about 3 K [21–24]. Pressure has also revealed further complexities of this system’s superconducting state, with multiple superconducting order parameters appearing

[21,24–26]. It was shown that above a critical pressure $p_c \simeq 1.5 - 1.7$ GPa, magnetic order occurs with the concomitant disappearance of superconductivity [21–26]. Several studies combining pressure and high magnetic field have been performed. When a magnetic field is applied along the a axis (the easy axis at ambient pressure) the multiple superconducting states have quite different behaviors [25]. Under a magnetic field $\mathbf{H} \parallel \mathbf{b}$, the metamagnetic field decreases strongly with pressure and superconductivity remains stacked below H_m [22]. For $\mathbf{H} \parallel \mathbf{c}$, a large enhancement of H_{c2} was found with an inversion of the anisotropy of H_{c2} in the $\mathbf{b} - \mathbf{c}$ plane for pressures close to p_c [22]. We note that a recent study showed that the magnetic anisotropy is significantly changed with pressure, with \mathbf{b} becoming the easy magnetic axis above p_c [27]. In addition, re-entrant superconductivity occurs for $\mathbf{H} \parallel \mathbf{c}$ just above the critical pressure [28], and the re-entrant superconducting phase induced in a magnetic field tilted by 30° from \mathbf{b} towards \mathbf{c} is expanded under pressure [29]. The above high-pressure studies were performed in static magnetic fields, mostly limited to fields below about 30 T. The study in Ref. [29] was performed up to 45 T, which is the highest static field available worldwide today. But even this is insufficient to reveal all the physics in UTe_2 , as known from the ambient pressure studies made in pulsed magnetic fields to much higher values. These studies were performed under pressures $p < 2$ GPa and those in high magnetic fields were limited to temperatures $T < 5$ K [25,29], $T < 10$ K [23,28], $T < 20$ K [22], and $T < 50$ K [26]. Here we report on an experiment combining high pressure and pulsed magnetic fields. We probed the behavior of UTe_2 over a wider experimental window than in the previous works: magnetic fields up to 60 T were combined with temperatures ranging up to at least 60 K and pressures up to >3 GPa. This allowed us to characterize the different nonsuperconducting phases and regimes, giving new insight into the evolution of the magnetic properties and their feedback on superconductivity in three-dimensional (3D) (H, p, T) phase diagrams. In particular, a Fermi-liquid description shows that the enhancement of the coefficient A of the electrical resistivity, which is presumably controlled by critical magnetic fluctuations, coincides with a more robust superconductivity near the critical pressure.

II. METHODS

We used a previously described pressure cell [30] allowing magnetoresistivity measurements in pulsed magnetic fields up to 60 T and temperatures down to 1.4 K. Single crystals of UTe_2 were grown by the chemical vapor transport technique as described elsewhere [2]. The crystals were oriented by x-ray Laue diffraction and cut to bar shaped samples of about $0.8 \times 0.2 \times 0.1$ mm³. Two successive experiments were performed in a pressure cell, offering the simultaneous measurement of the electrical resistivity of two samples in a magnetic field along the \mathbf{b} and \mathbf{c} directions. A first experiment was performed at pressures above p_c on samples $\#A$ with $\mathbf{H} \parallel \mathbf{b}$ and $\#B$ with $\mathbf{H} \parallel \mathbf{c}$ (see Supplemental Material [31]). A second experiment was performed under a large set of pressures below and above p_c , from 0.3 to 3.1 GPa, on samples $\#C$ with $\mathbf{H} \parallel \mathbf{b}$ and $\#D$ with $\mathbf{H} \parallel \mathbf{c}$, and corresponds to the data presented in this paper (see also Supplemental Material [31]).

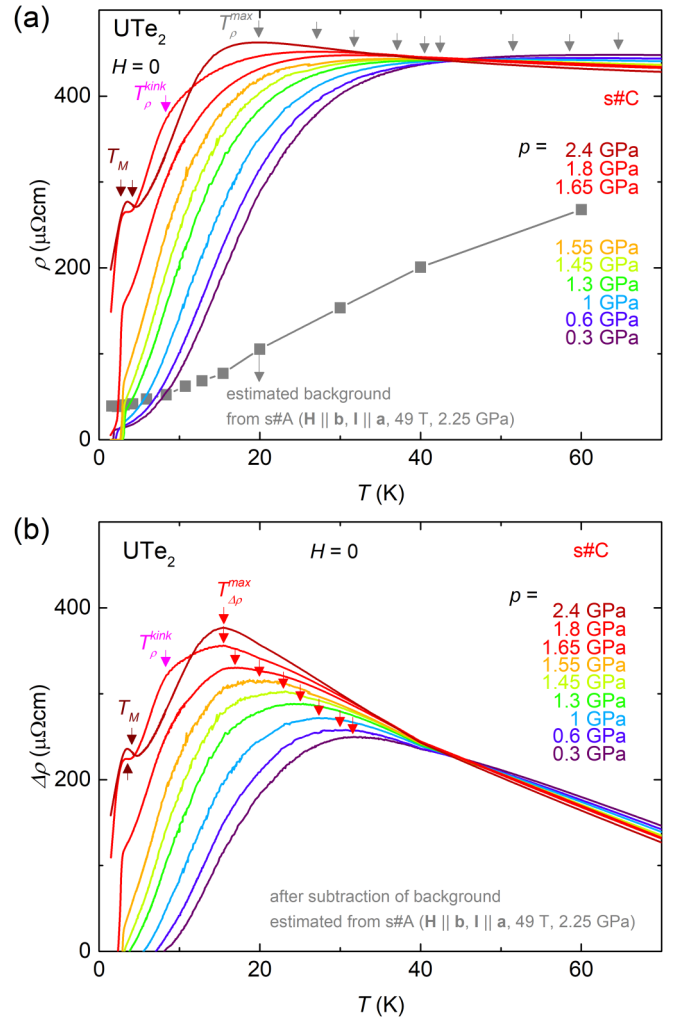


FIG. 1. (a) Zero-field temperature-dependence of the electrical resistivity ρ of UTe_2 under pressure. The grey squares show the curve at high pressure and high field that we take as a background. (b) Temperature dependence of resistivity $\Delta\rho$ determined after subtraction of the background.

Both experiments gave similar results, although the sample $\#C$ set up for $\mathbf{H} \parallel \mathbf{b}$ displayed an unintentional misalignment (see Sec. III), probably having moved on pressurization. A piece of lead was also mounted in the cell to determine the pressure. High-pressure magnetoresistivity measurements were performed at the Laboratoire National des Champs Magnétiques Intenses (LNCMI) in Toulouse under long-duration (50 ms rise and 300 ms fall) pulsed magnetic fields up to 58 T and temperatures down to 1.4 K. A standard four-probe method with a current $\mathbf{I} \parallel \mathbf{a}$ of 0.5 mA, at a frequency of 15–70 kHz and digital lock-in detection was used. The temperature dependence of the resistivity was also measured directly in zero field.

III. RESULTS

A. Zero-field high-pressure properties

Zero-field electrical resistivity $\rho(T)$ curves measured at different pressures are shown in Figs. 1(a) and 1(b). For

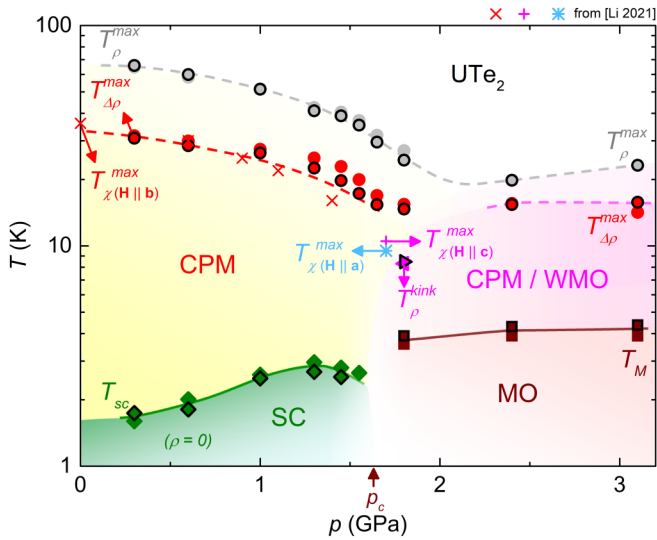


FIG. 2. Phase diagram of UTe_2 from these and previous measurements. CPM and CPM/WMO denote the correlated paramagnetic regimes stabilized at pressures below and above p_c , respectively, SC the superconducting phase, and MO the magnetically-ordered phase. One-color and black-border full symbols correspond to samples $\#C$ and $\#D$, respectively. Crosses were obtained from magnetic susceptibility measurements in [27].

pressures up to 1.55 GPa, superconductivity indicated by zero resistivity is apparent at low temperatures. For pressures of 1.8 GPa and above, a different anomaly appears in the resistivity curve (labeled T_M) that is almost certainly the signature of long-range magnetic order. In our study the critical pressure p_c lies between these values. In the 1.8 GPa curve a further anomaly is apparent at higher temperature (T_ρ^{kink}). A similar anomaly has been seen in other resistivity studies at pressures just above p_c [23,24] and a broad anomaly is also visible in the magnetization [27]. Another feature of the $\rho(T)$ curves is a broad maximum, which occurs at a temperature $T_\rho^{\text{max}} \simeq 60$ K at ambient pressure. T_ρ^{max} decreases with pressure down to about 20 K at $p \simeq 2$ GPa, i.e., slightly above p_c , and then slightly shifts to higher temperatures again as pressure is further increased. This maximum in the electrical resistivity ρ , as well as a broad maximum also observed, at a temperature T_χ^{max} , in the magnetic susceptibility χ , are general features of heavy fermion systems. T_χ^{max} indicates the temperature scale below which a crossover between a high temperature paramagnetic (PM) state to a coherent heavy fermion state or correlated paramagnetic (CPM) state occurs.

In Fig. 2 we show the zero-field pressure-temperature phase diagram constructed from our measurements together with data from previous studies [27]. The superconducting critical temperature T_{sc} increases from an initial value of 1.7 K up to a maximum value of about 3 K at a pressure of about 1.3 GPa. T_{sc} then decreases abruptly and disappears at a critical pressure $p_c \simeq 1.6 - 1.7$ GPa. Reported values of p_c vary, probably due to different pressure conditions, ranging from about 1.4 to 1.7 GPa [21–28]. An interesting feature is the maximum in the susceptibility observed at the temperature T_χ^{max} for $\mathbf{H} \parallel \mathbf{b}$ below p_c [1,3,22,27]. T_ρ^{max} and T_χ^{max} show similar behavior with pressure up to p_c , although their values

are quite different. Of course, neither feature is a precise indication of this energy scale, which is anyway a crossover, but the large temperature difference here is due to the effect of other contributions to the resistivity, including (but not limited to) phonon scattering, which should be subtracted to get the magnetic scattering. The temperature shift induced by this effect can be quite significant in the case of UTe_2 , as the maximum is rather broad and weak. To check, we subtracted the background shown in Fig. 1(a), corresponding to a $\rho(T)$ curve obtained under combined high pressure and magnetic field. This background corresponds to a high-field regime where the ground state is magnetically polarized. The curve selected for the background, obtained on sample $\#A$ for a magnetic field $\mu_0\mathbf{H} \parallel \mathbf{b}$ of 49 T and a pressure $p = 2.25$ GPa (see Supplemental Material [31]), corresponds to the case with the lowest resistivity in the temperature range (10–40 K) where the contribution of the magnetic correlations to the resistivity is predominant, implying that a significant part of these have been suppressed. Although this choice is of course somewhat arbitrary, empirically we see that, once the background is subtracted, the maximum is much more pronounced and occurs at a temperature $T_{\Delta\rho}^{\text{max}}$ quite close to T_χ^{max} , which delimitates the CPM regime [see Figs. 1(b) and 2]. Knowing that it is also possible to follow the maximum in $\Delta\rho$ to high fields as will be shown later, we therefore conclude that $T_{\Delta\rho}^{\text{max}}$ is a good criterion to follow the crossover to the CPM regime as a function of pressure, field and temperature. Beyond the critical pressure, a switch of the magnetic properties is observed, in relation with the onset of long-range magnetic ordering (MO), and possibly higher-temperature correlated paramagnetism or short-range weak magnetic ordering (noted CPM/WMO, see later): A maximum in the magnetic susceptibility is observed for $\mathbf{H} \parallel \mathbf{a}, \mathbf{c}$ at the temperatures $T_\chi^{\text{max}}(\mathbf{H} \parallel \mathbf{a})$ and $T_\chi^{\text{max}}(\mathbf{H} \parallel \mathbf{c})$, respectively, but no maximum of the magnetic susceptibility is observed for $\mathbf{H} \parallel \mathbf{b}$ [27].

B. High-field and high-pressure electrical resistivity

In Figs. 3(a) and 3(b) we show the magnetoresistivity curves at the lowest temperature (1.4 K) for different pressures and the two magnetic-field orientations. Most of the main results of this study are already apparent here. For the sample set up with $\mathbf{H} \parallel \mathbf{b}$, at low pressure the first-order metamagnetic transition appears as a huge and sharp increase of the resistivity, similar to what is seen at ambient pressure. However, here at 0.3 GPa this occurs at $\mu_0 H_m \simeq 43$ T, a field significantly higher than at ambient pressure (about 35 T) whereas it has previously been shown that H_m decreases with pressure [22,27]. The most likely explanation for this discrepancy is that the sample was somewhat misaligned in respect to the field, probably having moved inside the pressure cell on pressurization. Indeed, it has been shown that H_m increases when the field is rotated away from the $\mathbf{b} - \mathbf{c}$ and $\mathbf{b} - \mathbf{a}$ planes [6]. The value of H_m found here would imply quite a large misalignment, between 15° and 30° . However, as the effect of a magnetic field up to 35 T applied along the \mathbf{b} axis has already been well studied [22,26], we will see that this tilted configuration allows us to capture the essential physics for $\mathbf{H} \parallel \mathbf{b}$, as well as revealing interesting results for a field applied with some misalignment from the \mathbf{b} axis. In the

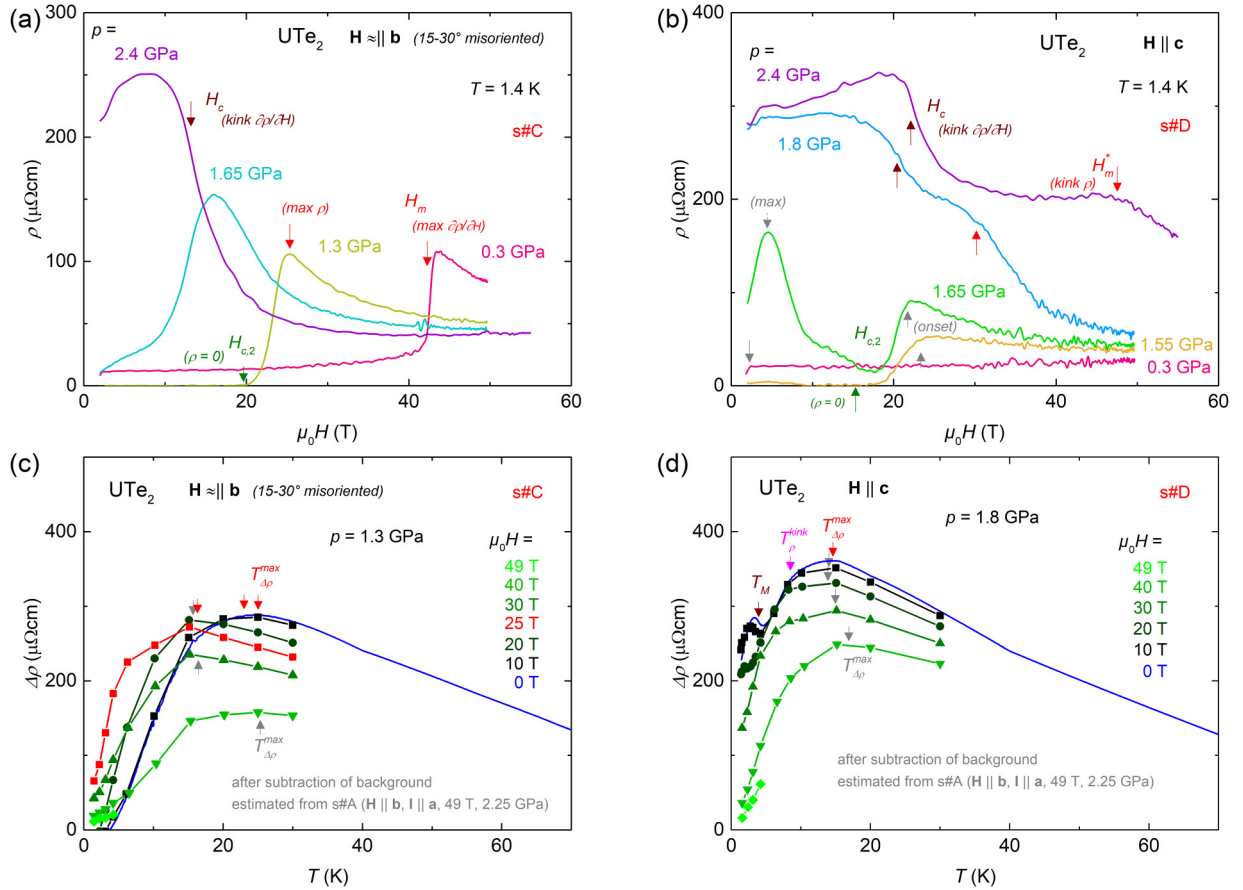


FIG. 3. Magnetoresistivity $\rho(H)$ curves at different pressures and at the lowest temperature (1.4 K) for the configurations (a) $\mathbf{H} \approx \parallel \mathbf{b}$ and (b) $\mathbf{H} \parallel \mathbf{c}$. Reconstructed temperature dependence of the resistivity $\Delta\rho$ determined after subtraction of the background under magnetic field (c) $\mathbf{H} \approx \parallel \mathbf{b}$ at 1.3 GPa and (d) $\mathbf{H} \parallel \mathbf{c}$ at 1.8 GPa (2b).

following we will refer to this field configuration as $\mathbf{H} \approx \parallel \mathbf{b}$. On increasing pressure, the metamagnetic transition remains clear up to p_c where H_m decreases to about 12 T. At higher pressure the aspect of the curve changes and shows several features that we will explicit further on. For the sample with $\mathbf{H} \parallel \mathbf{c}$ the resistivity curve is basically featureless at 0.3 GPa, similar to the ambient pressure results [8]. In the high pressure curves (1.8 and 2.4 GPa), the zero-field resistivity at 1.4 K has increased considerably, and shows a decrease with field in two steps with the corresponding field values marked here as H_c and H_m^* . Concerning the superconductivity, the lowest temperature reached in this paper (1.4 K) is only slightly below the ambient pressure superconducting critical temperature, so at low pressures we see almost no trace of superconductivity. However, T_{sc} increases significantly with pressure, and our measurements give a good indication of the superconducting phase diagram. Two important effects are visible here. First for $\mathbf{H} \approx \parallel \mathbf{b}$, we see that at 1.3 GPa, superconductivity extends up to $\mu_0 H_m \simeq 20$ T. At ambient pressure, it has been shown that for a field perfectly aligned along the b -axis, superconductivity is reinforced with field and exists up to H_m , but that this effect disappears with a misalignment of just a few degrees, and H_{c2} is considerably reduced. With the misalignment necessary to explain the large value of H_m in our case we would certainly not expect superconductivity to extend up to H_m at ambient pressure, so this implies that pressure strongly

changes the phase diagram when the field is rotated away from the b axis. The second remarkable effect is seen for $\mathbf{H} \parallel \mathbf{c}$, where at 1.55 GPa the resistivity is not zero at low fields, but a re-entrant superconducting state with zero resistivity is found at high field, between approximately 8 and 18 T, similar to the previous reports (Ref. [28] for $\mathbf{H} \parallel \mathbf{c}$ and Ref. [23] for an undetermined field direction).

A fuller understanding of the above effects and the complex phase diagram can be obtained by looking in detail at the temperature dependence of the magnetoresistivity. First, we examine the case for $\mathbf{H} \approx \parallel \mathbf{b}$. Figure 4 (left-hand graphs) shows the resistivity curves for different temperatures and three pressures. For $p = 1$ and 1.55 GPa, i.e., $p \lesssim p_c$, the curves are qualitatively similar to the ambient pressure results [8]. At low temperature, the first-order metamagnetic transition to the polarized paramagnetic (PPM) regime appears as a sharp and large increase of the resistivity. As temperature is increased this anomaly transforms into a broad maximum indicating a crossover delimiting the CPM regime. H_m decreases with pressure as mentioned previously, and apart from the larger value of H_m due to the misalignment of the field our results are similar to the previous study under pressure for $\mathbf{H} \parallel \mathbf{b}$ [22]. $\rho(T)$ curves are extracted at different field values from our $\rho(H)$ data collected at constant temperatures under pulsed magnetic field. The background subtraction described in Sec. III A permits to follow the maximum in $\Delta\rho$ and

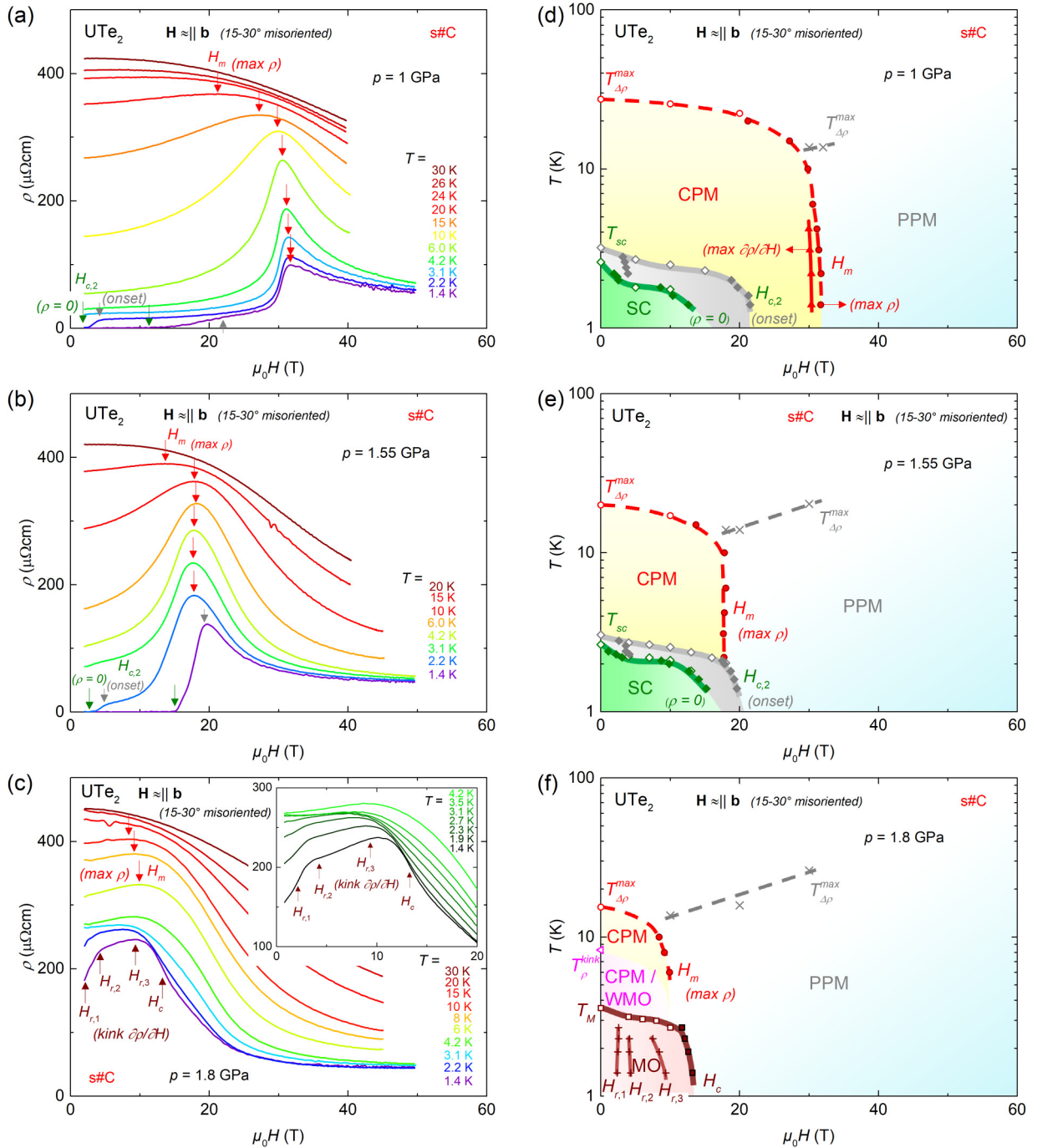


FIG. 4. Left-hand graphs: Magnetoresistivity curves for the configuration $\mathbf{H} \approx \parallel \mathbf{b}$ at different temperatures for the pressures (a) $p = 1$ GPa, (b) $p = 1.55$ GPa, and (c) $p = 1.8$ GPa. Right-hand graphs: Obtained magnetic-field-temperature phase diagrams of the superconducting and magnetically ordered phases, and of the CPM regime delimited by H_m and $T_{\Delta\rho}^{\text{max}}$, for the pressures (d) $p = 1$ GPa, (e) $p = 1.55$ GPa, and (f) $p = 1.8$ GPa. CPM and CPM/WMO denote the correlated paramagnetic regimes stabilized at pressures below and above p_c , PPM the polarized paramagnetic regime, SC the superconducting phase, and MO the magnetically-ordered phase. Red circles and pink triangles delimit the CPM and CPM/WMO regimes, green diamonds the SC phase, and brown squares the MO phase. Open symbols and grey crosses were extracted from $\rho(T)$ curves while full symbols and brown crosses were extracted from $\rho(H)$ curves.

to extract the associated temperature $T_{\Delta\rho}^{\text{max}}$ in high magnetic fields. Figure 3(c) shows $\Delta\rho(T)$ measured at different fields up to 49 T and at the pressure $p = 1.3$ GPa (data at other pressures are shown in the Supplemental Material [31]). The phase diagrams drawn from these anomalies are shown in the right-hand panels of Fig. 4. The field where the maximum

of the resistivity occurs decreases as pressure is increased, similarly to the ambient pressure results [8], and connects with the temperature $T_{\chi(\mathbf{H}\parallel\mathbf{b})}^{\text{max}}$ that also decreases with pressure [22,27]. We can see that the temperature $T_{\Delta\rho}^{\text{max}}$ at the maximum of the zero-field resistivity after subtraction of the background described above, which corresponds approximately to T_{χ}^{max} at

zero field, also corresponds to H_m in the range where both features can be seen. This implies that $T_{\Delta\rho}^{\max}$ is indeed a good criterion to determine the boundary of the CPM regime. The superconducting phase diagrams are also plotted for $p = 1$ and 1.55 GPa. For both pressures H_{c2} shows an S shape, which may be due to the probable misalignment of field. As already mentioned, at 1.55 GPa superconductivity extends up to H_m as expected for $\mathbf{H} \parallel \mathbf{b}$ [22,26]. These results will be discussed in more detail further on. The lower panels of Fig. 4 show the results for $\mathbf{H} \approx \parallel \mathbf{b}$ at 1.8 GPa. The high temperature magnetoresistivity curves retain the characteristic broad maximum seen at pressures below p_c , indicating a crossover into a polarized state. This maximum disappears at temperatures above 10-15 K, corresponding to the value of $T_{\Delta\rho}^{\max}$, and becomes a broad decrease of the resistivity with field. However, the magnetoresistivity curves at low temperature are quite different. Now $p > p_c$ and the ground state is almost certainly some kind of long-range magnetic order below $T_M \simeq 3$ K. For $T < T_M$ a pronounced kink can be seen at $\mu_0 H_c \simeq 13$ T corresponding to the transition from the long-range magnetic order to the polarized paramagnetic state. Several other features are visible in the magnetoresistivity at the fields $\mu_0 H_{r,1} = 2.3$ T, $\mu_0 H_{r,2} = 4.3$ T, and $\mu_0 H_{r,3} = 9.3$ T $< \mu_0 H_c$ at $T = 1.4$ K. These transitions are presumably related to magnetic moment reorientations within the magnetically ordered phase (see Supplemental Material [31]).

We now look at the case $\mathbf{H} \parallel \mathbf{c}$ (Fig. 5). For this configuration no metamagnetic transition has been observed at ambient pressure at least up to 70 T [5,8]. For the pressures 1.3 and 1.55 GPa, i.e., $p \lesssim p_c$, at high temperatures no particular feature is apparent in the magnetoresistivity. The temperature $T_{\Delta\rho}^{\max}$ at the maximum of $\Delta\rho$, from the background subtraction described in Sec. III A, slightly increases with magnetic field, see Fig. 3(d) for $p = 1.8$ GPa and the Supplemental Material [31] for other sets of data, which indicates that the change from the CPM into the PPM regime is very progressive. The most interesting result here concerns the superconductivity. At ambient pressure the $H_{c2}(T)$ curve for $\mathbf{H} \parallel \mathbf{c}$ shows no enhancement of superconductivity with field. However several studies have already shown that under pressure the situation changes, with the slope of H_{c2} becoming extremely steep [21,22], possibly indicating the appearance of a field-enhancement of superconductivity for $\mathbf{H} \parallel \mathbf{c}$, and re-entrant superconductivity appearing close to the critical pressure. These effects are confirmed here: the upper and middle panels of Fig. 5 show that $\mu_0 H_{c2}$ reaches about 20 T at 1.3 GPa and that re-entrant superconductivity develops at 1.55 GPa, where $\mu_0 H_{c2}$ exceeds 20 T, respectively. The lower panels of Fig. 5 show that at 1.8 GPa, i.e., for $p > p_c$, the critical field H_c where the low-temperature long-range magnetic order is destroyed can be seen as a well-defined kink in the curves for temperatures below $T_M \simeq 3$ K. At the lowest temperature the critical field reaches $\mu_0 H_c \simeq 20$ T and it shifts slightly to lower field as the temperature increases. Similarly to the $\mathbf{H} \approx \parallel \mathbf{b}$ configuration, three anomalies in the electrical resistivity can be defined at the critical fields $\mu_0 H_{r,1} = 2.8$ T, $\mu_0 H_{r,2} = 8.1$ T, and $\mu_0 H_{r,3} = 12.3$ T $< \mu_0 H_c$ at $T = 1.4$ K, within the magnetically ordered state (see Supplementary Materials [31]). As for the configuration $\mathbf{H} \approx \parallel \mathbf{b}$, all these features disappear when the temperature is raised above T_M ,

confirming their link to the low-temperature magnetic order. However, for $p > p_c$, in contrast to the $\mathbf{H} \approx \parallel \mathbf{b}$ configuration a pronounced kink remains at higher field suggesting a transition or a well-defined crossover into the polarized state. We denote this field H_m^* and speculate on its pseudo-metamagnetic nature, in analogy with the metamagnetic field where the polarized state occurs at low pressure for $\mathbf{H} \approx \parallel \mathbf{b}$, although here it does not show a sharp first-order transition. The nature of the regime between H_c and H_m^* is not clear. Anomalies have previously been seen in the resistivity, the specific heat and the magnetization [24,27] at a temperature higher than T_M for pressures close above p_c . Indeed, in the present paper a clear kink can be seen at the temperature $T_{\rho}^{\text{kink}} \simeq 8.5$ K in the zero-field resistivity at 1.8 GPa (Fig. 3). It has been suggested that this phase could correspond to static [24] or short-range [27] weak magnetic order (WMO). The field H_m^* probably corresponds to a transition or crossover between this phase and the polarized paramagnetic regime. Interestingly, a maximum in the magnetic susceptibility was observed at a temperature $T_{\chi(\mathbf{H}\parallel\mathbf{c})}^{\max} = 11$ K for a pressure $p = 1.8$ GPa $> p_c$ and a magnetic field $\mathbf{H} \parallel \mathbf{c}$ [27]. Similarly to the low-pressure CPM regime delimited in a magnetic field $\mathbf{H} \parallel \mathbf{b}$ by $T_{\chi(\mathbf{H}\parallel\mathbf{b})}^{\max}$ and H_m [4,8] (see also other heavy-fermion systems [32,33]), the WMO regime may also correspond to a second CPM regime delimited in a magnetic field $\mathbf{H} \parallel \mathbf{c}$ by $T_{\chi(\mathbf{H}\parallel\mathbf{c})}^{\max}$ and H_m^* . In the following, we will label this regime as CPM/WMO.

C. Magnetic quantum criticality and superconductivity

The full 3D phase diagrams obtained for both configurations of magnetic field $\mathbf{H} \approx \parallel \mathbf{b}$ and $\mathbf{H} \parallel \mathbf{c}$ are represented in Fig. 6. We see that the phase diagram for the magnetic order is quite similar for both configurations, with the ordering temperature being suppressed with field, but with a well-defined transition even at high field. A similar behavior has also been seen for \mathbf{H} applied along the easy magnetic axis \mathbf{a} , where the critical field is even smaller [25]. The succession of field-induced transitions at fields $H_{r,i} < H_c$, with $i = 1 - 3$, (presented in Figs. 4 and 5, but not in Fig. 6 for clarity) indicates the stabilization of different magnetic structures. Such behavior would not be expected for a ferromagnetically-ordered phase, at least for a field applied along the easy axis, strongly suggesting that the magnetic order is of an antiferromagnetic (or spin-density-wave) type, as already inferred from previous results [21,22,24,25].

A switch of polarization processes occurs at p_c and leads to quite different 3D phase diagrams for the two configurations $\mathbf{H} \approx \parallel \mathbf{b}$ and $\mathbf{H} \parallel \mathbf{c}$:

(i) At pressures below p_c , for $\mathbf{H} \approx \parallel \mathbf{b}$ the CPM regime appears as a well-defined 3D bubble, delimited by the first-order transition at H_m at low temperature and the temperature $T_{\Delta\rho}^{\max}$ (or T_{χ}^{\max}) at low field. However, for $\mathbf{H} \parallel \mathbf{c}$, while at zero field the crossover between the low-temperature CPM and high-temperature paramagnetic regimes is obviously the same, there is no signature of transition to the PPM regime with field, and it is likely that a change develops smoothly as a continuous rotation of the moments. This is consistent with the absence of a maximum in the magnetic susceptibility for $\mathbf{H} \parallel \mathbf{c}$, which is almost Curie-Weiss-like down to the lowest

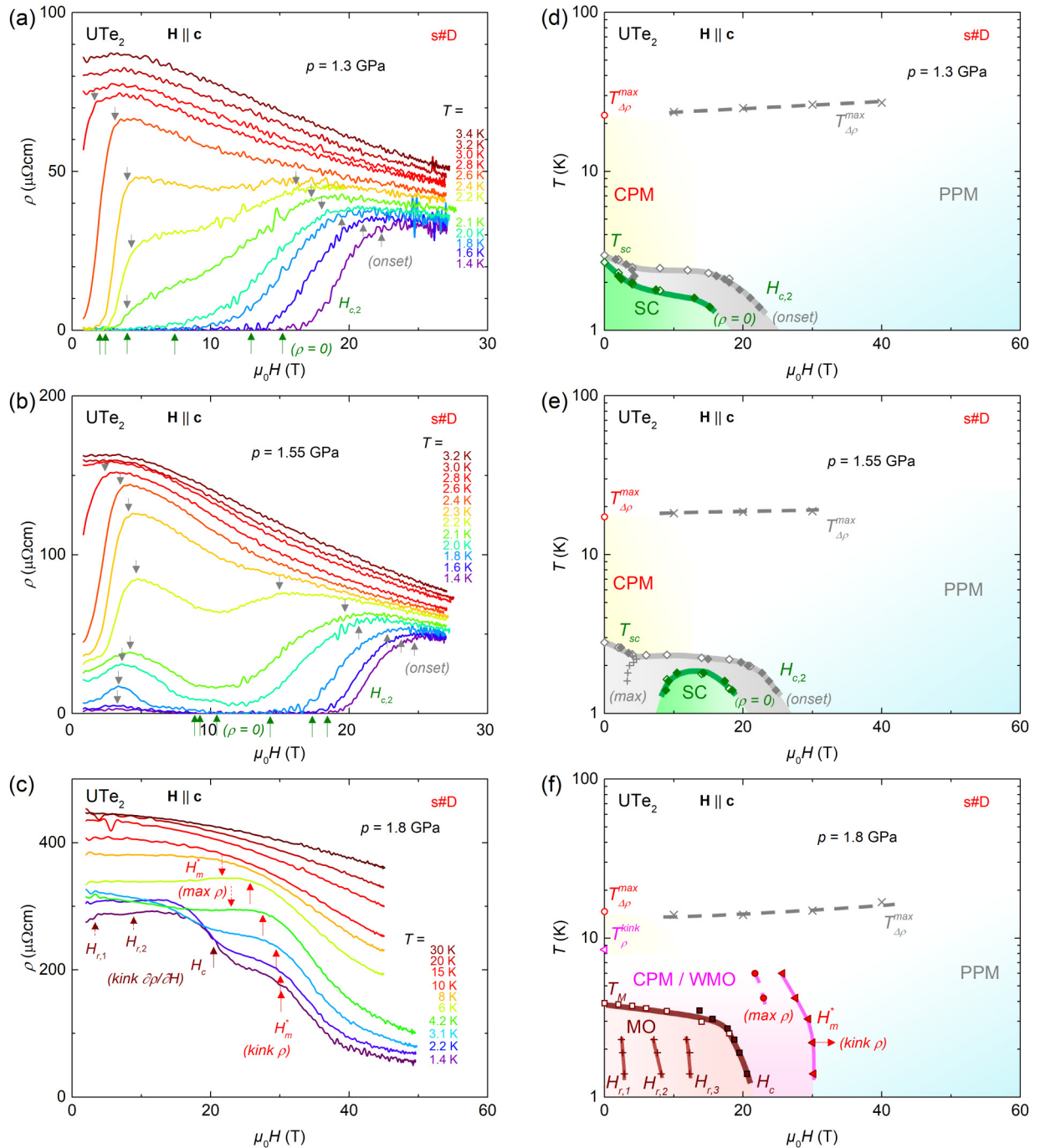


FIG. 5. Left-hand graphs: Magnetoresistivity curves for the configuration $\mathbf{H} \parallel \mathbf{c}$ at different temperatures for the pressures (a) $p = 1.3$ GPa, (b) $p = 1.55$ GPa, and (c) $p = 1.8$ GPa. Right-hand graphs: Obtained magnetic-field-temperature phase diagrams of the superconducting and magnetically ordered phases, and of the CPM regime delimited by H_m and $T_{\Delta\rho}^{\text{max}}$, for the pressures (d) $p = 1.3$ GPa, (e) $p = 1.55$ GPa, and (f) $p = 1.8$ GPa. CPM and CPM/WMO denote the correlated paramagnetic regimes stabilized at pressures below and above p_c , PPM the polarized paramagnetic regime, SC the superconducting phase, and MO the magnetically-ordered phase. Red circles and triangles delimit the CPM and CPM/WMO regimes, green diamonds the SC phase, and brown squares the MO phase. Open symbols and grey crosses were extracted from $\rho(T)$ curves while full symbols and brown crosses were extracted from $\rho(H)$ curves.

temperatures [3,10], and with the fact that $T_{\Delta\rho}^{\text{max}}$ increases with applied field for $\mathbf{H} \parallel \mathbf{c}$.

(ii) For pressures above p_c the situation is quite different. Now a 3D bubble formed by the CPM/WMO regime occurs for $\mathbf{H} \parallel \mathbf{c}$, with a quite well-defined transition into the PPM regime, whereas for $\mathbf{H} \approx \parallel \mathbf{b}$ this probably occurs as a broad

crossover. This is also consistent with the appearance of a maximum of magnetic susceptibility for $\mathbf{H} \parallel \mathbf{c}$ and the disappearance of such maximum for $\mathbf{H} \parallel \mathbf{b}$ under pressures beyond p_c [27].

This reshuffling of the magnetic properties at the critical pressure p_c is related to a switch of the anisotropy of the mag-

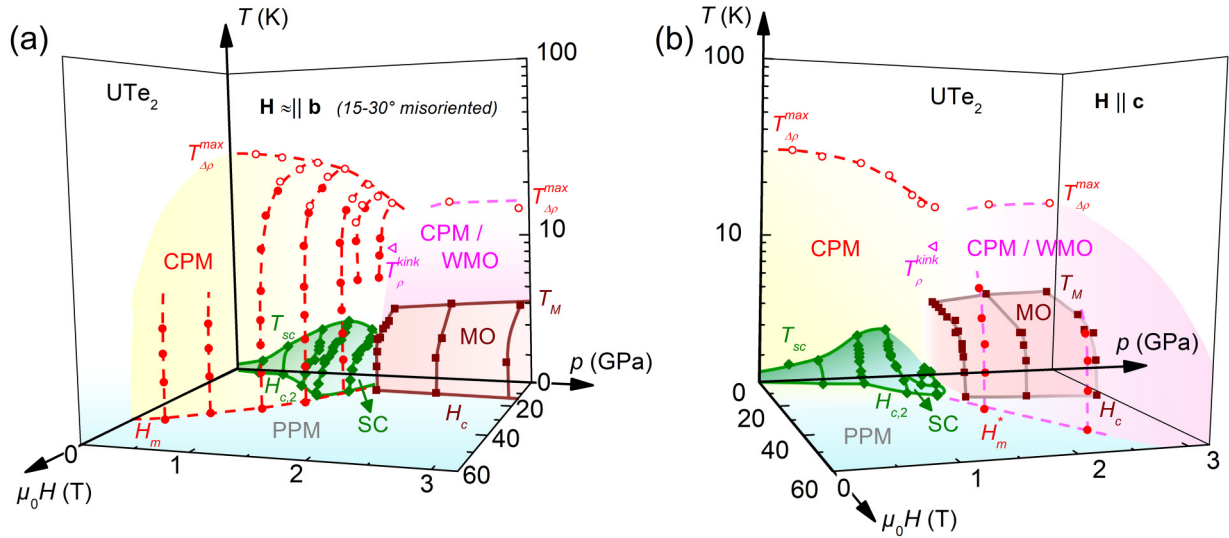


FIG. 6. 3D magnetic-field-pressure-temperature phase diagrams for the configurations (a) $\mathbf{H} \approx \parallel \mathbf{b}$ and (b) $\mathbf{H} \parallel \mathbf{c}$. In both diagrams, $T = 1.4$ K is the lower temperature of the vertical scales. CPM and CPM/WMO denote the correlated paramagnetic regimes stabilized at pressures below and above p_c , PPM the polarized paramagnetic regime, SC the superconducting phase, and MO the magnetically-ordered phase. Red circles delimit the CPM and CPM/WMO regimes, brown squares the MO phase, and green diamonds the SC phase.

netic susceptibility, with the hard magnetic axis \mathbf{b} at ambient pressure becoming the easy magnetic axis at high pressure [27].

In heavy-fermion materials, magnetic quantum criticality, generally accompanied by a Lifshitz Fermi-surface instability, is reflected in the enhancement of the effective mass m^* as the field is increased towards H_m seen by a direct measurement of the specific heat [34], as well as from magnetization [4] and resistivity [8] measurements. Magnetic fluctuations are often considered as the origin of the large effective mass m^* observed in these materials [33]. The quadratic temperature coefficient A , obtained by a fit of the resistivity to a Fermi-liquid behavior $\rho = \rho_0 + AT^2$, varies as m^{*2} within first approximation and shows a pronounced maximum at H_m for $\mathbf{H} \parallel \mathbf{b}$, as well for a field tilted by 30° in the $\mathbf{b} - \mathbf{c}$ plane [10]. In Fig. 7 we show the field dependence of the A coefficient for different pressures, extracted from the reconstructed temperature dependencies of the resistivity for both configurations. For the configuration $\mathbf{H} \approx \parallel \mathbf{b}$, at the lowest pressures the metamagnetic transition appears as a very sharp peak at H_m , starting at about 43 T at 0.3 GPa. As pressure is increased the peak position moves to lower fields, the value of A increases, and above 1.3 GPa the peak starts to broaden noticeably. For the highest pressures ($p > p_c$) the low field ($H < H_c$) points are omitted as the onset of magnetic order occurring close to the lowest temperature measured here made the analysis meaningless in this case. For the configuration $\mathbf{H} \parallel \mathbf{c}$, at low pressure no feature is visible in $A(H)$. However, above 1 GPa a broad maximum becomes apparent that shifts to higher fields and becomes more pronounced as pressure is increased, remaining visible even for $p > p_c$.

The considerable changes of the magnetic properties with pressure have strong consequences on the superconductivity. In the 3D phase diagrams of Fig. 6, an enhancement of superconductivity can be seen close to p_c for both configurations of magnetic field $\mathbf{H} \approx \parallel \mathbf{b}$ and $\mathbf{H} \parallel \mathbf{c}$. Previous studies have

shown that field re-entrant superconductivity develops at ambient pressure and low temperature for a sample perfectly aligned with $\mathbf{H} \parallel \mathbf{b}$ and that, at a temperature of 1.4 K, the sample should be superconducting at all fields up to H_m once a small pressure is applied [7,22]. Here, due to misalignment, no re-entrant superconductivity is seen for $\mathbf{H} \approx \parallel \mathbf{b}$ at low pressure and H_{c2} is quite low at $T = 1.4$ K. However, we find that superconductivity extends up to H_m as pressure is increased. We observed the same phenomenon in a first experiment with sample $\sharp A$ close to p_c (see Supplemental Material [31]). This sample, also set up for $\mathbf{H} \parallel \mathbf{b}$, was not measured at low pressure, so we have no direct indication of its misalignment if any, but it is unlikely that this would be exactly the same as for sample $\sharp C$. All these results suggest that the phenomenon of superconductivity extending up to H_m under pressure is rather robust and true for fields applied over a quite large angular range around the b axis. Concerning the configuration $\mathbf{H} \parallel \mathbf{c}$, we have evidenced the presence of field-induced superconductivity under pressures $p \lesssim p_c$. The lower panels [(c)–(d)] of Fig. 7 show the electronic (p, H) phase diagrams at our base temperature, $T = 1.4$ K, with the evolution of A as a color plot. They emphasize the relationship between the enhancement of A and the high-field stabilization of superconductivity. Field-reinforced or field-induced superconductivity is observed close to the critical pressure, where the collapse of the field scales H_m and H_m^* and enhanced A coefficients are observed. For $\mathbf{H} \approx \parallel \mathbf{b}$ superconductivity survives up to H_m under pressures near to p_c , where A reaches its maximum value at H_m . For $\mathbf{H} \parallel \mathbf{c}$ and $p = 1.55$ GPa, although no field-induced magnetic transition is observed at temperatures larger than T_{sc} , superconductivity may result from the proximity of critical magnetic fluctuations, as indicated by the enhancement of A in a nearby region of the phase diagram. A is maximum near H_m^* for $p \gtrsim p_c$, and the field-induced superconducting phase, which develops for $p \lesssim p_c$ appears as a prolongation of the H_m^* line.

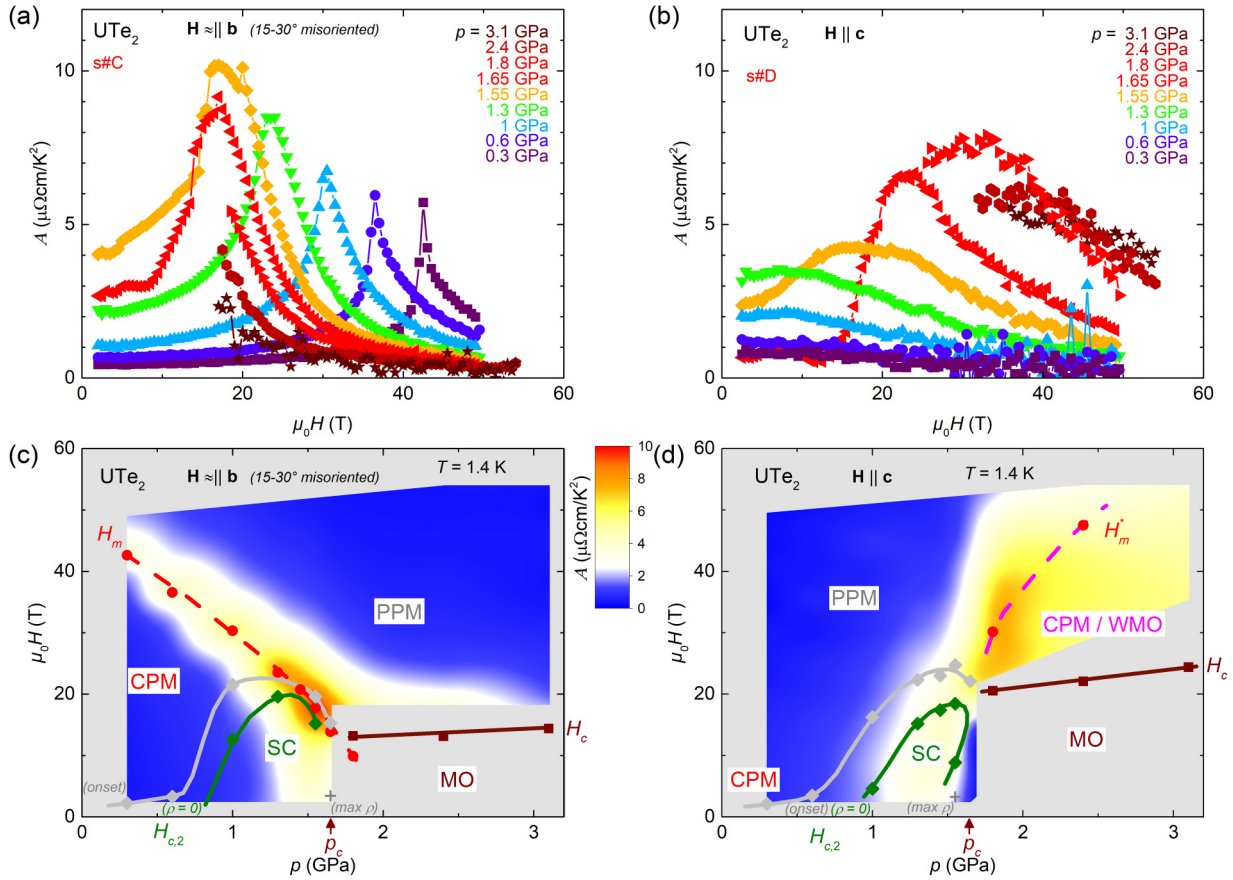


FIG. 7. Top graphs: Field dependence of the quadratic temperature dependence coefficient A at different pressures for the configurations (a) $\mathbf{H} \approx \parallel \mathbf{b}$ and (b) $\mathbf{H} \parallel \mathbf{c}$. Lower graphs [(c)–(d)]: Color plot of A with superimposed pressure-magnetic-field phase diagrams showing how, for both configurations, the enhancement of superconductivity coincides with an enhancement of A . The coefficient A was not determined within the grey regions.

IV. DISCUSSION

Quantum criticality, either purely magnetic or accompanied by a Fermi-surface instability, is suspected to be a driving force for superconductivity in many heavy-fermion systems. In UTe_2 this is evidenced by the enhancement of superconductivity on approaching the magnetic phase transition under pressure, and on approaching metamagnetic transitions with field. For the latter case, a quantitative analysis has shown that the re-entrant superconducting behavior for $\mathbf{H} \parallel \mathbf{b}$ can be explained by a monotonic increase of the pairing strength related to the increase of the effective mass m^* [7,35]. Furthermore, the rapid disappearance of the re-entrant behavior as soon as the field is rotated away from the b axis is a natural consequence, mainly due to the increase of H_m . Indeed, as the enhancement of the pairing strength occurs at higher fields, it is no longer sufficient to overcome the orbital and possibly paramagnetic pair-breaking effects at lower fields. A small anisotropy of the Fermi velocity can further amplify this phenomenon. From this picture, it is easy to understand our result. As can be seen from the $A(H)$ curves, as pressure is increased the enhancement of m^* and consequently of the pairing strength will simultaneously occur at lower fields and become stronger, allowing the field enhancement of superconductivity to be effective over a much wider angular range. We

expect that, with a measurement made at lower temperatures, we would have found a superconducting state extending up to H_m at even lower pressure. An open question is whether on approaching p_c the field enhancement of superconductivity is still effective or not. In a previous study with $\mathbf{H} \parallel \mathbf{b}$, the characteristic S shape of H_{c2} was lost for pressures above 1 GPa [22]. The initial slope remained large but H_{c2} showed a pronounced curvature that could be an indication of increasingly effective Pauli limitation with pressure. In the present paper, for $\mathbf{H} \approx \parallel \mathbf{b}$ we see the S shape of H_{c2} at 1.55 GPa implying that the field reinforcement effect might still be active. This is consistent with the pressure and field dependence of A , which still shows a pronounced maximum at H_m , and reaches higher values than at ambient pressure. The difference between the present and previous studies is probably due to the misalignment here, leading to higher values of H_m for a given pressure. Indeed at $p = 1.55$ GPa we find $\mu_0 H_m \simeq 18$ T, which corresponds approximately to the value found at $p = 1$ GPa for the field perfectly aligned $\mathbf{H} \parallel \mathbf{b}$ [22,26]. A probable scenario is therefore that the field enhancement of superconductivity as $H \rightarrow H_m$ is always present, but is more pronounced and leads to the S shape when H_m is large. What is clear from the study with configuration $\mathbf{H} \approx \parallel \mathbf{b}$ is that the metamagnetic transition at H_m still acts as a very effective cut-off for superconductivity, which does not survive in the polarized state. This is similar to

the ambient pressure behavior for $\mathbf{H} \parallel \mathbf{b}$ but now concerns a wider angular range. It contrasts with the surprising re-entrant superconducting phase only seen in the PPM regime stabilized above H_m in the configuration with a magnetic field H tilted by 30° from \mathbf{b} toward \mathbf{c} at ambient pressure [6,10]. Recently a study performed in this configuration under pressure showed that superconductivity extends continuously below and above H_m [29]. It seems that here we are not in this configuration, implying that we probably have also a component of field along the a axis, and so the extension of superconductivity up to H_m may be found also for misalignment of the field in the $\mathbf{a} - \mathbf{b}$ plane under pressure.

For $\mathbf{H} \parallel \mathbf{c}$, the extremely steep slope found for H_{c2} on approaching p_c , as well as the very high values (25 – 30 T) found for H_{c2} here and in a previous study [28], strongly suggest that pressure causes an enhancement of the superconducting pairing strength to come into play. Figure 7 shows clearly how this enhancement seems to be linked to the maximum of $A(H)$ that appears under pressure, and thus to the new field scale H_m^* , corresponding to the crossover to the polarized state from the CPM/WMO state. Approaching p_c we find a re-entrant behavior of superconductivity as has been reported previously [28]. While the field enhancement of the pairing strength is certainly favorable for this re-entrant behavior, the main ingredient is probably the competition between the magnetically ordered and superconducting phases. Indeed previous studies (in a magnetic field along \mathbf{c} [28] or along an undetermined direction [23]) showed that superconductivity only appears above the field necessary to suppress the magnetic order. This would suggest that in the present paper the measurement at 1.55 GPa is actually at a pressure slightly above p_c . For $\mathbf{H} \parallel \mathbf{c}$ and close to p_c , a question is whether superconductivity can develop in the correlated or polarized paramagnetic regimes, or in both.

Interestingly, the electrical resistivity ρ measured here with a current $\mathbf{I} \parallel \mathbf{a}$ captures the physics driving the maxima in the magnetic susceptibility for different directions of magnetic field. Figure 2 shows the similar values of $T_{\Delta\rho}^{\max}$ and $T_{\chi(\mathbf{H}\parallel\mathbf{b})}^{\max}$ for $p < p_c$, and of $T_{\Delta\rho}^{\max}$ and $T_{\chi(\mathbf{H}\parallel\mathbf{a})}^{\max} \simeq T_{\chi(\mathbf{H}\parallel\mathbf{c})}^{\max}$ for $p \gtrsim p_c$ [27]. The development of magnetic fluctuations was observed in several heavy-fermion systems at temperatures $T \lesssim T_{\chi}^{\max}$, T_{ρ}^{\max} and may drive the maxima in ρ and χ (see Refs. [32,33] and Refs. therein). Antiferromagnetic fluctuations were also found to vanish in the prototypical heavy-fermion paramagnets CeRu_2Si_2 and CeCu_6 in fields beyond their metamagnetic field H_m [36], where a CPM regime is replaced by a polarized paramagnetic (PPM) regime with a large magnetization $M \gtrsim 1 \mu_B$. In many systems, this picture of a CPM regime controlled by intersite magnetic fluctuations is supported by the relation $T_{\chi}^{\max} \sim H_m \sim \Gamma$ between its boundaries T_{χ}^{\max} and H_m and the relaxation rate Γ of antiferromagnetic fluctuations [33]. In the light of recent

inelastic neutron scattering experiments [17,18], the picture of a CPM regime controlled by magnetic fluctuations may be relevant for UTe_2 at ambient pressure too. Further, a transverse relationship between the electrical resistivity and the magnetic susceptibility anisotropies may be the consequence of an anisotropic Kondo hybridization between conduction and localized f electrons in UTe_2 . Rich information about the electronic interactions responsible for the magnetic fluctuations in UTe_2 in its normal nonsuperconducting phases may be accessed via a careful investigation of the anisotropy of the electrical resistivity, with different electrical-current directions (see [37]), under different magnetic-field directions possibly combined with pressure.

We have seen that the application of pressure and high magnetic field on UTe_2 leads to an extremely complex phase diagram with a complete reshuffling of the magnetic anisotropy and strong associated effects on superconductivity. This helps us understand the intricate relationship between superconductivity and magnetism in this system. The clear signature of the destruction of magnetic order with field, as well as the signature of several field induced transitions inside the magnetically ordered phase, show that this order may be of antiferromagnetic or SDW type. Different domains of stability and exclusion of superconductivity are found under pressure and magnetic fields. Critical magnetic fluctuations, possibly of ferromagnetic kind, associated with H_m and H_m^* , may induce the large values of A observed here, in relation with the enhancement of the superconducting pairing mechanism. However, superconductivity does not necessarily occur in all parts of the phase diagram where A is enhanced. Quite simple pictures can explain some parts of the phase diagram, but understanding why superconductivity is destroyed below or beyond a metamagnetic field, depending on the field direction, and in the magnetically-ordered phase stabilized under pressure remains a theoretical challenge. Experimentally, a full knowledge of the angle dependence of superconductivity under pressure and very high magnetic field would help gaining a full understanding of superconductivity in UTe_2 . Our study is a step in this direction.

ACKNOWLEDGMENTS

We thank J. Flouquet and J.-P. Brison for useful discussions. We acknowledge financial support from the Cross-Disciplinary Program on Instrumentation and Detection of CEA, the French Alternative Energies and Atomic Energy Commission, KAKENHI (JP15H05882, JP15H05884, JP15K21732, JP16H04006, JP15H05745, JP19H00646, JP19K03736) and GIMRT (19H0416, 19H0414), and the French national research agency Programme Investissements d’Avenir under Program No. ANR-11-IDEX-0002-02, Reference No. ANR-10-LABX-0037-NEXT, and the collaborative research project FRESCO.

[1] S. Ran, C. Eckberg, Q.-P. Ding, Y. Furukawa, T. Metz, S. R. Saha, I.-L. Liu, M. Zic, H. Kim, J. Paglione, and N. P. Butch, *Science* **365**, 684 (2019).

[2] D. Aoki, A. Nakamura, F. Honda, D. Li, Y. Homma, Y. Shimizu, Y. J. Sato, G. Knebel, J.-P. Brison, A. Pourret *et al.*, *J. Phys. Soc. Jpn.* **88**, 043702 (2019).

- [3] S. Ikeda, H. Sakai, D. Aoki, Y. Homma, E. Yamamoto, A. Nakamura, Y. Shiokawa, Y. Haga, and Y. Onuki, *J. Phys. Soc. Jpn.* **75**, 116 (2006).
- [4] A. Miyake, Y. Shimizu, Y. J. Sato, D. Li, A. Nakamura, Y. Homma, F. Honda, J. Flouquet, M. Tokunaga, and D. Aoki, *J. Phys. Soc. Jpn.* **88**, 063706 (2019).
- [5] A. Miyake, Y. Shimizu, Y. J. Sato, D. Li, A. Nakamura, Y. Homma, F. Honda, J. Flouquet, M. Tokunaga, and D. Aoki, *J. Phys. Soc. Jpn.* **90**, 103702 (2021).
- [6] S. Ran, I.-L. Liu, Y. S. Eo, D. J. Campbell, P. Neves, W. T. Fuhrman, S. R. Saha, C. Eckberg, H. Kim, J. Paglione *et al.*, *Nat. Phys.* **15**, 1250 (2019).
- [7] G. Knebel, W. Knafo, A. Pourret, Q. Niu, M. Vališka, D. Braithwaite, G. Lapertot, M. Nardone, A. Zitouni, S. Mishra *et al.*, *J. Phys. Soc. Jpn.* **88**, 063707 (2019).
- [8] W. Knafo, M. Vališka, D. Braithwaite, G. Lapertot, G. Knebel, A. Pourret, J.-P. Brison, J. Flouquet, and D. Aoki, *J. Phys. Soc. Jpn.* **88**, 063705 (2019).
- [9] Q. Niu, G. Knebel, D. Braithwaite, D. Aoki, G. Lapertot, M. Vališka, G. Seyfarth, W. Knafo, T. Helm, J.-P. Brison, J. Flouquet, and A. Pourret, *Phys. Rev. Research* **2**, 033179 (2020).
- [10] W. Knafo, M. Nardone, M. Vališka, A. Zitouni, G. Lapertot, D. Aoki, G. Knebel, and D. Braithwaite, *Commun. Phys.* **4**, 40 (2021).
- [11] F. Lévy, I. Sheikin, B. Grenier, and A. D. Huxley, *Science* **309**, 1343 (2005).
- [12] D. Aoki, T. D. Matsuda, V. Taufour, E. Hassinger, G. Knebel, and J. Flouquet, *J. Phys. Soc. Jpn.* **78**, 113709 (2009).
- [13] B. Wu, G. Bastien, M. Taupin, C. Paulsen, L. Howald, D. Aoki, and J.-P. Brison, *Nat. Commun.* **8**, 14480 (2017).
- [14] Y. Tokunaga, D. Aoki, H. Mayaffre, S. Krämer, M.-H. Julien, C. Berthier, M. Horvatić, H. Sakai, S. Kambe, and S. Araki, *Phys. Rev. Lett.* **114**, 216401 (2015).
- [15] S. Sundar, S. Gheidi, K. Akintola, A. M. Côté, S. R. Dunsiger, S. Ran, N. P. Butch, S. R. Saha, J. Paglione, and J. E. Sonier, *Phys. Rev. B* **100**, 140502(R) (2019).
- [16] C. Paulsen, G. Knebel, G. Lapertot, D. Braithwaite, A. Pourret, D. Aoki, F. Hardy, J. Flouquet, and J.-P. Brison, *Phys. Rev. B* **103**, L180501 (2021).
- [17] C. Duan, K. Sasmal, M. B. Maple, A. Podlesnyak, J.-X. Zhu, Q. Si, and P. Dai, *Phys. Rev. Lett.* **125**, 237003 (2020).
- [18] W. Knafo, G. Knebel, P. Steffens, K. Kaneko, A. Rosuel, J.-P. Brison, J. Flouquet, D. Aoki, G. Lapertot, and S. Raymond, *Phys. Rev. B* **104**, L100409 (2021).
- [19] C. Duan, R. E. Baumbach, A. Podlesnyak, Y. Deng, C. Moir, A. J. Breindel, M. B. Maple, and P. Dai, [arXiv:2106.14424](https://arxiv.org/abs/2106.14424).
- [20] S. Raymond, W. Knafo, G. Knebel, K. Kaneko, J.-P. Brison, J. Flouquet, D. Aoki, and G. Lapertot, *J. Phys. Soc. Jpn.* **90**, 113706 (2021).
- [21] D. Braithwaite, M. Vališka, G. Knebel, G. Lapertot, J.-P. Brison, A. Pourret, M. E. Zhitomirsky, J. Flouquet, F. Honda, and D. Aoki, *Commun. Phys.* **2**, 147 (2019).
- [22] G. Knebel, M. Kimata, M. Vališka, F. Honda, D. Li, D. Braithwaite, G. Lapertot, W. Knafo, A. Pourret, Y. J. Sato, Y. Shimizu, T. Kihara, J.-P. Brison, J. Flouquet, and D. Aoki, *J. Phys. Soc. Jpn.* **89**, 053707 (2020).
- [23] S. Ran, H. Kim, I.-L. Liu, S. R. Saha, I. Hayes, T. Metz, Y. S. Eo, J. Paglione, and N. P. Butch, *Phys. Rev. B* **101**, 140503(R) (2020).
- [24] S. M. Thomas, F. B. Santos, M. H. Christensen, T. Asaba, F. Ronning, J. D. Thompson, E. D. Bauer, R. M. Fernandes, G. Fabbri, and P. F. S. Rosa, *Sci. Adv.* **6**, eabc8709 (2020).
- [25] D. Aoki, F. Honda, G. Knebel, D. Braithwaite, A. Nakamura, D. Li, Y. Homma, Y. Shimizu, Y. J. Sato, J.-P. Brison, and J. Flouquet, *J. Phys. Soc. Jpn.* **89**, 053705 (2020).
- [26] W. C. Lin, D. J. Campbell, S. Ran, I.-L. Liu, H. Kim, A. H. Nevidomskyy, D. Graf, N. P. Butch, and J. Paglione, *npj Quantum Mater.* **5**, 68 (2020).
- [27] D. Li, A. Nakamura, F. Honda, Y. J. Sato, Y. Homma, Y. Shimizu, J. Ishizuka, Y. Yanase, G. Knebel, J. Flouquet, and D. Aoki, *J. Phys. Soc. Jpn.* **90**, 073703 (2021).
- [28] D. Aoki, M. Kimata, Y. J. Sato, G. Knebel, F. Honda, A. Nakamura, D. Li, Y. Homma, Y. Shimizu, W. Knafo, D. Braithwaite, M. Vališka, A. Pourret, J.-P. Brison, and J. Flouquet, *J. Phys. Soc. Jpn.* **90**, 074705 (2021).
- [29] S. Ran, S. R. Saha, I.-L. Liu, D. Graf, J. Paglione, and N. P. Butch, *npj Quantum Mater.* **6**, 75 (2021).
- [30] D. Braithwaite, W. Knafo, R. Settai, D. Aoki, S. Kurahashi, and J. Flouquet, *Rev. Sci. Instrum.* **87**, 023907 (2016).
- [31] See Supplemental Material at <http://link.aps.org/supplemental/10.1103/PhysRevB.104.214507> for complementary graphs show details about the electrical-resistivity data accumulated on four samples, and how they were analyzed to extract the phase diagrams and the evolution of the Fermi-liquid coefficient A .
- [32] D. Aoki, W. Knafo, and I. Sheikin, *C. R. Phys.* **14**, 53 (2013).
- [33] W. Knafo, Habilitation à Diriger des Recherches (University of Toulouse, 2021), Chap. 3, [arXiv:2107.13458](https://arxiv.org/abs/2107.13458).
- [34] S. Imajo, Y. Kohama, A. Miyake, C. Dong, M. Tokunaga, J. Flouquet, K. Kindo, and D. Aoki, *J. Phys. Soc. Jpn.* **88**, 083705 (2019).
- [35] J.-P. Brison (to be published).
- [36] J. Rossat-Mignod, L. Regnault, J. Jacoud, C. Vettier, P. Lejay, J. Flouquet, E. Walker, D. Jaccard, and A. Amato, *J. Magn. Magn. Mater.* **76-77**, 376 (1988).
- [37] Y. S. Eo, S. R. Saha, H. Kim, S. Ran, J. A. Horn, H. Hodovanets, J. Collini, W. T. Fuhrman, A. H. Nevidomskyy, N. P. Butch, M. S. Fuhrer, and J. Paglione, [arXiv:2101.03102](https://arxiv.org/abs/2101.03102).